ARTICLE   OPEN

Highly selective phonon diffusive scattering in superionic layered AgCrSe$_2$

Chen Wang[1,2] and Yue Chen [1,2]✉

Superionic materials that exhibit coexistence of rigid crystalline lattices and liquid-like fluctuating substructures have emerged as promising thermoelectric materials. The inadequate understanding of the phonon behavior in the superionic state, however, still prevents further revealing of the underlying correlation between the thermally induced liquid-like atomic dynamics and anomalous thermal transport properties. Herein, by adopting a hybrid scheme to directly characterize anharmonic phonon quasiparticles from ab-initio molecular dynamics, we manifest that low-energy transverse phonons dominated by Ag atoms totally collapse, whereas longitudinal optical phonons remain largely intact during the superionic transition. The ultralow thermal conductivity originates from the atomic level structural heterogeneity can be ultimately attributed to diffusive phonon dynamics. Our study also reveals that the extremely large selective phonon diffusive scattering can be counteracted by hydrostatic pressure induced deactivation of the liquid-like flow of Ag atoms. These results demonstrate the decisive role of ion superionicity in phonon scattering across superionic transition and may pave the way for new phonon engineering strategies in related superionic materials.

INTRODUCTION

The thermal conduction of condensed systems can be considered as microscopic atomic diffusion among equilibrium positions, where the averaged rearrangement time serve as an intrinsic criterion to distinguish solid from liquid[1,2]. Compared with negligible diffusive time in liquid, which enables the fluidity, the hopping time between well-defined lattice sites is enormous for crystalline solid. The hierarchically multi-layered superionic crystals, however, are rare materials exhibiting long range liquid-like ionic diffusivity while simultaneously maintaining solid crystalline sublattices. They have attracted steady interest with promising applications in fuel cells[3], solid rechargeable batteries electrolytes[4], and high-efficient thermoelectric materials[5–7] by virtue of the unique solid-liquid duality. In thermoelectric conversion, the efficiency is governed by a dimensionless figure of merit $zT = \alpha^2 T / \rho(\kappa_L + \kappa_e)$, where α is the Seebeck coefficient, T is the absolute temperature, ρ is the electrical resistivity, κ_L is the lattice thermal conductivity, and κ_e is the carrier thermal conductivity. The Weidemann–Franz law: $\kappa_e \rho = LT$, where L is the constant Lorenz number, indicates that any attempt to lower κ_e will enhance the ρ, which ultimately deteriorates the zT. Therefore, without an increase in ρ, substantial efforts have been invested to suppress the phonon propagation to reduce the κ_L to a glass-like value[8–10].

The concept of phonon-liquid electron-crystal (PLEC)[6], which evolved from phonon-glass electron-crystal (PGEC)[11], postulates that the lattice thermal conductivity can be tremendously inhibited by disrupting the propagation of transverse acoustic phonons in superionic crystals, characterized by the conception that fluid does not sustain shear stress. Accordingly, the remarkable combination of the intrinsic nature of long range liquid-like ion diffusivity within the crystalline sublattice and the versatile chemical variability of the layered structure make the intercalated superionic crystal a potential candidate to realize the PLEC concept and a high-performance thermoelectric material.

More essentially, the relationship between the exceptional thermal transport and superionic atomic dynamics remains controversial and elusive in such layered systems, owing to the lack of a suitable anharmonic phonon-based description[12–15]. Although, recent studies have revealed that the ultralow thermal conductivity could be closely related to the breakdown of the transverse acoustic (TA) modes[6,12,16–18], it has also been argued that the low-energy rattling optical modes could play a vital role in thermal conductivity suppression[8,12]. Therefore, an in-depth investigation of the superionic diffusive response of the individual phonon modes is of great importance to better understand the phonon scattering mechanism behind the liquid-like thermal conduction.

The layered AgCrSe$_2$ superionic compound exhibits ultralow liquid-like thermal conductivity with $\kappa_L \sim 0.5$ Wm^{-1}K^{-1} above the critical transition temperature (T_c) of around 450 K[12,19] and has a unity thermoelectric figure of merit zT at about 800 K[20]. The thermally induced reversible superionic phase transition, which has been ascribed to the oscillated Ag$^+$ ions in quasi-two-dimensional (2D) potential wells[13], provides an opportunity to study the phonon evolution across the order-disorder transition. Although, diverse phonon scattering frameworks have been proposed to account for the liquid-like thermal conductivity[12,16,21], a detailed microscopic mechanism is yet to be fully unveiled due to the lack of mode-based anharmonic phonon calculations and corresponding momentum-resolved inelastic neutron scattering (INS) measurements on single crystals. Herein, instead of adopting the three-phonon scattering mechanism to account for the anharmonicity of liquid-like ions, which could severely underestimate the acoustic phonon average relaxation time due to its incapability in dealing with layered diffusive systems[22,23], an effective hybrid scheme[24,25] has been applied to directly characterize anharmonic phonon quasiparticles from ab-initio molecular dynamics (AIMD) simulations. For well-defined phonon quasiparticle (i.e., a single peak with a Lorentzian line shape in

[1]Department of Mechanical Engineering, The University of Hong Kong, Pokfulam Road, Hong Kong SAR, China. [2]HKU Zhejiang Institute of Research and Innovation, 1623 Dayuan Road, 311305 Lin An, China. ✉email: yuechen@hku.hk

power spectrum), this approach has been proven effective regardless of the structure complexity in modest size supercells[26–28]. Our AIMD simulations reveal that acoustic phonons predominately involved with Ag contributions are selectively scattered, while longitudinal optical phonons remain well-defined in superionic state. Moreover, our results indicate that the diffusive scattering originates from thermally induced liquid-like Ag flow can be counterbalanced by hydrostatic pressure, which may provide an alternative for further phonon engineering.

RESULTS

The crystal structure of $AgCrSe_2$ is hexagonal layered with two possible tetrahedral sites in Ag intercalated layer, which sandwiched by octahedral layers of $CrSe_6$, as shown in Fig. 1a. At low temperature, only one of the tetrahedral sites is fully occupied by Ag^+ ions, and the structure has a $R3m$ symmetry. Below Néel transition temperature $T_N \sim 55$ K, the Cr^{3+} magnetic moment reaches 2.58 μ_B and stack antiferromagnetically along c axis[13]. As temperature rises, an order-disorder transition has been observed across T_c, which redistributes the Ag^+ ions between two tetrahedral sites equivalently and changes the averaged structure symmetry to $R\bar{3}m$. The significant increase of ionic diffusivity across superionic transition has been first interpreted by calculating the root mean square displacement (RMSD) $\Delta(r)$, which often serves as an indicator of the solid-liquid phase transition[29]. As shown in Fig. 1b, $\Delta(r)_{Ag}$ plateau exists at $T \leq 300$ K, corresponding to characteristic solid vibrational behavior due to strong restoring force provided by the crystal binding. Upon heating to 400 K, however, the $\Delta(r)_{Ag}$ demonstrates a pronounced liquid-like diffusive behavior, which can be clearly seen from the $\sqrt{t}$ time dependence of $\Delta(r)_{Ag}$. Similar liquid-like diffusive patterns have also been observed for $T > 400$ K, where larger $\Delta(r)_{Ag}$ indicates stronger Ag flow. The dramatic transformation of RMSD between 300 K and 400 K, which is related to the ion diffusivity, well validates the superionic transition of Ag atoms[19]. The discrepancy between theoretical and experimental T_c may be related to the effects of limited supercell size in AIMD simulations[30].

In addition, the nature of the Ag thermal motion is quantified by analyzing the anisotropic displacement parameters (ADPs)[32] from AIMD simulations, as shown in Table 1. The estimated U_{11} is much larger than U_{33} for Ag atoms at 300 K, in reasonable agreement with previous Rietveld refinements of neutron powder diffraction patterns on $AgCrSe_2$, $U_{11} = 0.10$ and $U_{33} = 0.015$ Å^2 (ref. [12]). The ultralarge U_{11}, U_{22}, and U_{12} of Ag atoms at 400 K further reveal that the superionic mobility arises overwhelmingly from the in-plane (a-b plane) motions. As shown in Fig. 1c, in order to reveal the coexistence of liquid and solid states for different atomic species, the RMSD have also been calculated for Cr and Se atoms at 500 K. The difference of time dependence among $\Delta(r)_{Ag}$, $\Delta(r)_{Cr}$, and $\Delta(r)_{Se}$ indicates, instead of exhibiting liquid-like diffusive mobility, the Cr and Se atoms still maintain a solid vibrational characteristic. Additionally, the Ag self-diffusion constant calculated from Einstein's Brownian motion equation (i.e., $\Delta(r)_{Ag}^2 \sim t$) is $D = 9.6 \times 10^{-6}$ cm^2 s^{-1} at 500 K, which is comparable to the superionic Cu atom, $D = 7.2 \pm 0.4 \times 10^{-6}$ cm^2 s^{-1} at 495 K, obtained from neutron measurement on the analogous $CuCrSe_2$[16], further confirming the validity of our calculations.

To characterize the local structure changes during the superionic transition, the averaged total and partial pair distribution functions (PDF), $G(r)$, have been calculated from AIMD simulations, as shown in Fig. 2. Below T_c, the PDF for ordered crystalline solid exhibits well-defined peaks that broaden progressively as temperature increases, reflecting a more intensive thermal induced atomic vibration. The first pronounced total PDF peak is located at around 2.5 Å, which can be described as the superposition of the nearest neighbor Ag-Cr, Ag-Se, and Cr-Se correlations. The second peak (highlighted by a gray shaded bar), which is mainly contributed by non-Ag pairs (i.e., Cr-Cr and Se-Se), is less susceptible to the superionic transition, as indicated by the

Table 1. Anisotropic displacement parameters (Å^2) for Ag atoms across the superionic transition.

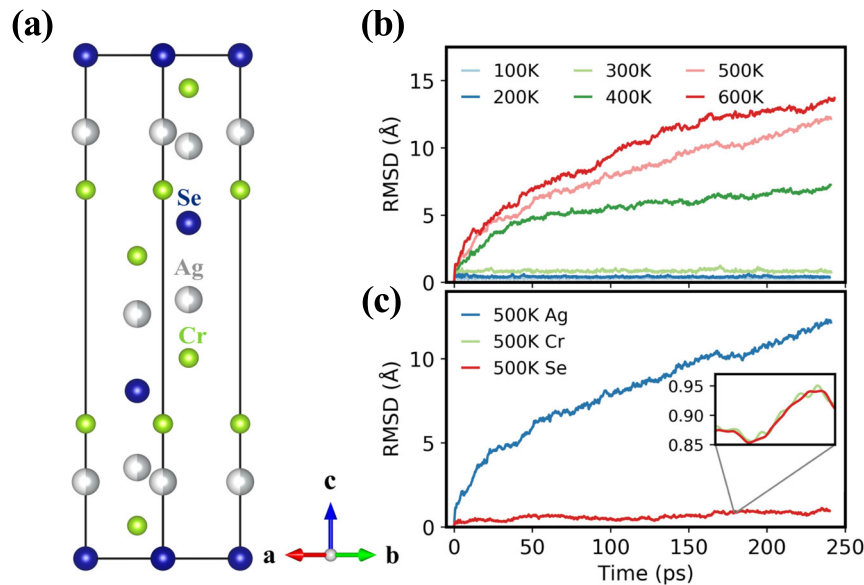|	U_{11}	U_{22}	U_{33}	U_{12}	U_{13}	U_{23}
300 K	0.148	0.155	0.021	0.078	0.001	0.004
400 K	7.032	9.024	0.087	0.608	0.040	0.058

Fig. 1 Crystal structure and superionic transition of $AgCrSe_2$. a The high-temperature crystal structure of $AgCrSe_2$ ($R\bar{3}m$ space group), which is visualized by VESTA[31]. The Ag atoms (indicated with half shadowed silver spheres) are equally distributed in two tetrahedral sites between $CrSe_6$ layers. **b** The RMSD of Ag at different temperatures. **c** The RMSD of Ag, Cr and Se at 500 K. The inset shows the amplified RMSD of Cr and Se atoms.

modest increase of the peak width across T_c. For Ag-dominated peaks (highlighted by a wheat shaded bar), however, they demonstrate a distinct critical-like behavior when $T > T_c$, as implied
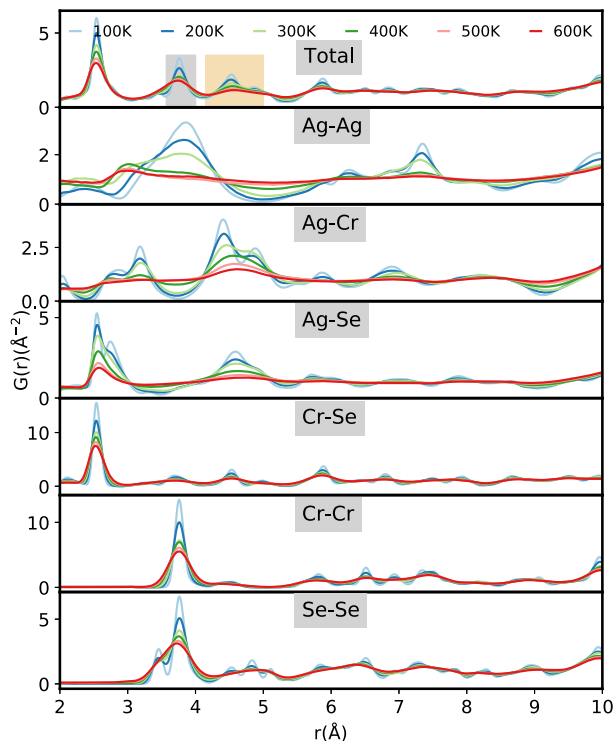

Fig. 2 Local structure evolution across the superionic transition of AgCrSe$_2$. Total PDF at different temperatures up to 10 Å as obtained from AIMD simulations and decomposed partial PDF for atomic pairs: Ag-Ag, Ag-Cr, Ag-Se, Cr-Se, Cr-Cr, and Se-Se. The vertical shaded bars highlight the Ag-poor (gray) and the Ag-rich (wheat) correlated areas.

by the drastic broadening of peak width, reflecting the loss of structural coherence induced by the activation of Ag superionic diffusion, consistent with previous neutron experiments on powder AgCrSe$_2$[12]. As shown in Ag-related partial PDF, a much liquid-like pattern has been observed above T_c, which implies that the Ag atoms are more evenly distributed within the quasi-2D potential wells after the order-disorder transition. The first peak of Ag-Ag pair, for instance, survives and shifts from 3.7 to 3.0 Å, which corresponds to the intermediate point of the two tetrahedral sites. Although the Ag-related PDF peaks broaden noticeably, Se and Cr dominated peaks show little change upon entering the superionic state, signifying the coexistence of CrSe$_6$ cages. Additionally, in the intermediate temperature range, above T_N but below T_c, jump diffusion between adjacent positions has also been observed, as seen from the merging of Ag-Cr (4.6 Å), Ag-Se (2.6 Å), and Se-Se (3.8 Å) peaks. The large vibrational amplitude at normal state can be attributed to the weak bonding provided by the breakdown of microscopic magnetic order of Cr^{3+} ions at elevated temperatures, in agreement with previous experimental findings[13].

The phonon power spectra are obtained by calculating the Fourier transform of the velocity autocorrelation function during AIMD simulations at the corresponding temperatures, as shown in Fig. 3(c). To determine different phonon modes, the phonon dispersion along high-symmetric directions has been calculated using finite difference method, as shown in Fig. 3(b). Definition of high-symmetric points of the primitive cell in the first Brillouin zone is illustrated in Fig. 3(a). It is seen from the temperature dependent power spectra that both transverse acoustic (TA) and longitudinal acoustic (LA) phonon peaks at around 0.78 THz and 2.40 THz are pronounced at low T, which then undergo gradual broadening upon heating from 100 to 300 K. Eventually, while the LA phonon softens noticeably as indicated by the shaded bar, the TA phonons almost collapse once the system transforms from normal state to superionic state. In order to further elucidate the individual phonon response at different regimes during the superionic transition, the mode-based spectra have been calculated at $q = (0.5, 0.5, 0.0)$ (i.e., zone boundary) and $q = (1/3, 1/3, 1/3)$ across T_c, as shown in Fig. 4. The calculated spectra show that TA
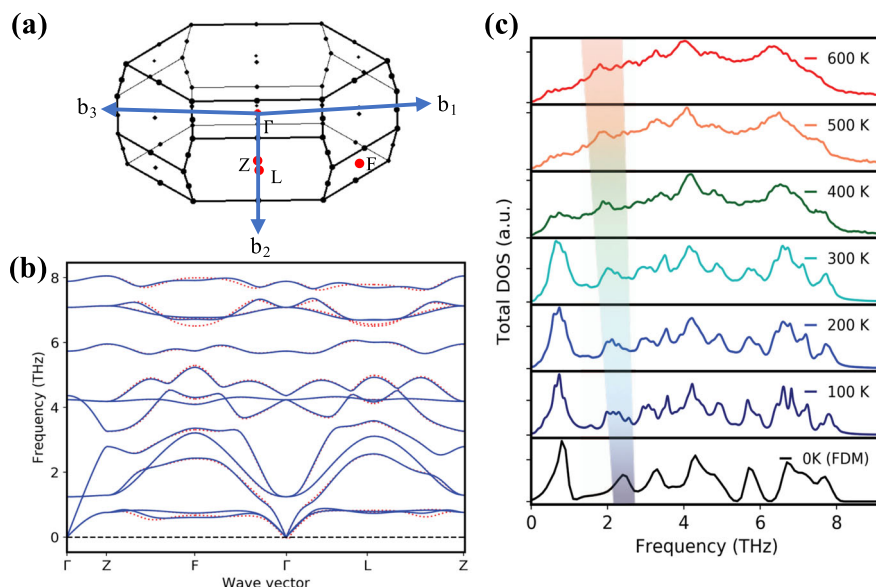

Fig. 3 Phonon dispersion and power spectra from simulations. a Schematic of high-symmetric points (red) in first Brillouin zone of primitive cell of AgCrSe$_2$. **b** The phonon dispersions of AgCrSe$_2$ calculated using $3 \times 3 \times 1$ (red) and $4 \times 4 \times 1$ (blue) supercells. **c** The phonon power spectra calculated at different temperatures from AIMD simulations. Density of states at 0 K was calculated from density functional theory (DFT) using finite difference method.
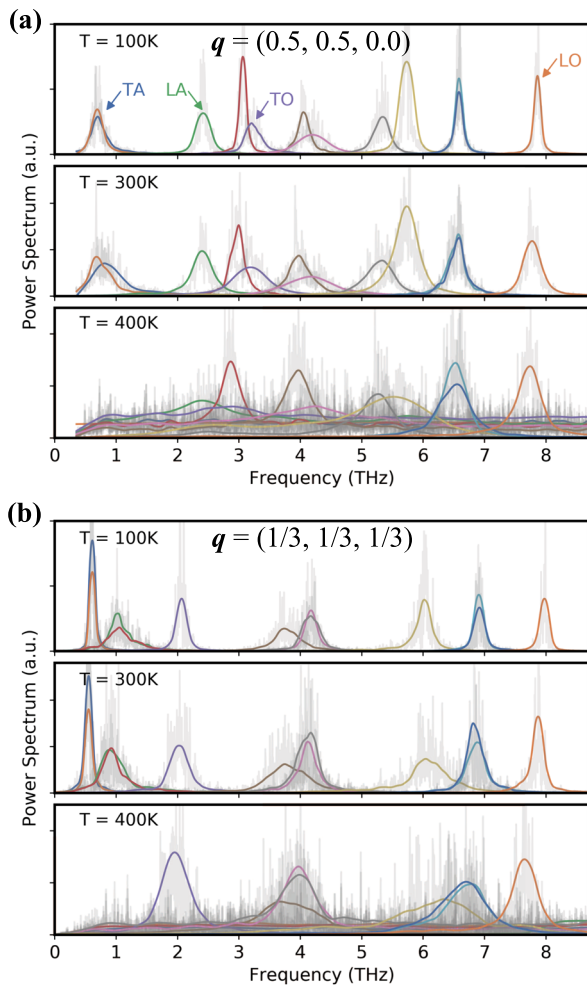
(a) T = 100K $q = (0.5, 0.5, 0.0)$

T = 300K

T = 400K

(b) T = 100K $q = (1/3, 1/3, 1/3)$

T = 300K

T = 400K

Fig. 4 Selective breakdown of Ag-dominated phonons. The normalized mode-projected power spectra of AgCrSe$_2$ at **a** q-vector (0.5, 0.5, 0.0) and **b** q-vector (1/3, 1/3, 1/3) at different temperatures calculated from AIMD simulations. The different colored solid curves represent the data convolved with locally weighted scatterplot smoothing (LOWESS) method with a bandwidth of 0.06 THz for the 12 phonon branches.

modes vanish in both specific dispersive and non-dispersive regimes in superionic state. In addition, the diffusive phonon scattering has demonstrated mode selectivity for optical phonons, whereas the transverse optical (TO) phonon at around 3.58 THz at $q = (0.5, 0.5, 0.0)$ broadens noticeably, the longitudinal optical (LO) phonon at 7.68 THz remains relatively unaffected to the disorder scattering of superionic Ag atoms. Furthermore, by analyzing the polarization vector of each normal mode, we found the collapsed TA phonons are overwhelmingly dominated by Ag vibrations, while the LA phonon arises from the collective vibrations of both Ag and Se atoms. The participation of Ag vibrations to those less affected optical phonons is also found to be insignificant and similar behavior has also been observed at $q = (0.0, 0.0, 0.0)$ (see the Supplemental Material). Recently, the INS measurements on single crystals of AgCrSe$_2$ suggest the persistence of dispersive TA phonons very close to the zone center, which could be also attributed to the contributions from Cr and Se atoms[33]. Additionally, the full width half maximum (Γ_T) of the Lorentzian fitted mode-based power spectra were calculated in frequency domain, which enables us to extract the critical phonon lifetime τ, using $\tau = 1/2\Gamma_T$. As a result of diffusive disorder, all TA phonons at $q = (0.5, 0.5, 0.0)$ breakdown completely and the lifetime of LA phonon (τ_{LA}) decreases from about 1.27 to 0.50 ps upon warming

from 300 to 400 K and remains nearly temperature independent afterwards as expected for alike partially liquidized materials[6,34].

To engineer the thermal properties through the manipulation of Ag diffusive motion, the hydrostatic pressure response of phonon has been investigated as well. Fig. 5a–c plots the simulated trajectory of atoms in the b-c plane of AgCrSe$_2$ at different temperatures and hydrostatic pressures. As one can see, above T_c, the Ag atoms delocalize between two tetrahedral sites, whereas at 300 K, only one tetrahedral site is occupied. It is found that, instead of showing delocalized liquid-like diffusion, the vibrational amplitude of Ag atoms becomes comparable to those of the Cr and Se atoms under pressure, indicating the Ag atoms are constrained around their equilibrium positions and the estimated U_{11} and U_{33} recover to 0.275 and 0.025 Å^2, respectively. The breakdown of the liquid-like structural heterogeneity is believed to be related to the increased bond strength between Ag atoms and the CrSe$_6$ cages with a decrease of bond length induced by the compressed lattice. As shown in Fig. 5(d), the Ag migrational energy barriers between two tetrahedral sites have been calculated using the climbing nudged elastic band (CI-NEB) method[35] under different hydrostatic pressures. By shifting atoms away from their equilibrium positions, we find that Ag atoms sit in a shallow potential well and are only weakly bonded on a-b plane at 0 GPa with a lattice diffusion barrier as low as 0.38 eV, leading to liquid-like ion mobility. However, the migration barrier increases to 0.63 eV while the pressure elevating from 0 to 10 GPa, which ultimately prevents the thermally induced fluid-like flow of Ag atoms at 400 K. The structure stability at high pressures is confirmed by the absence of imaginary frequencies in the phonon dispersion, as shown in Supplementary Fig. 7. The corresponding mode-projected power spectra of AgCrSe$_2$ at q-vector (0.5, 0.5, 0.0) and q-vector (1/3, 1/3, 1/3) for 400 K and 10 GPa have also been calculated, as shown in Fig. 5(e). We unveil that the diffusive scattering effect can be counteracted by the deactivation of superionic flow, as indicated by the re-emerging of TA phonons at low-frequency range.

DISCUSSION
In summary, we have explored the evolution of phonons in AgCrSe$_2$ across the superionic transition through AIMD simulations. From our theoretical results, we demonstrate the existence of atomic level structural heterogeneity. The specific low-energy Ag-dominated acoustic phonons collapse selectively, whereas longitudinal optical phonons that primarily involve octahedral CrSe$_6$ vibrations remain well-defined across the superionic transition. The thermally induced liquid-like flow can be deactivated by a hydrostatic pressure, which counteracts the superionic disorder phonon scattering. The insight obtained in this work into the phonon behavior in superionic crystals may pave the way for further phonon engineering of AgCrSe$_2$ and the related partially liquid-like materials.

METHODS
The harmonic phonon calculations were performed in the framework of DFT, as implemented in Vienna ab-initio simulation package (VASP)[36]. The Perdew–Burke–Ernzerhof generalized gradient approximation (GGA-PBE) functional was applied to account for the exchange-correlation of electrons[37]. The interaction between electrons and ions was described using the projector-augmented wave method (PAW)[38], with a plane wave cutoff energy of 500 eV. The configurations of Ag $4d^{10}5s^1$, Cr $3d^34s^2$, and Se $4s^24p^4$ were treated as valence electrons. We sampled the Brillouin zone with k-point meshes of $9 \times 9 \times 2$ for 12-atom hexagonal conventional cell and $3 \times 3 \times 1$ for the $4 \times 4 \times 1$ supercell. The collinear spin polarized calculation was performed with an energy convergence criterion of 10^{-8} eV. During the relaxation, the lattice parameters and atomic positions were fully optimized until atomic forces were smaller than 1 meV Å^{-1}. The phonon dispersion was obtained using the small displacement method as
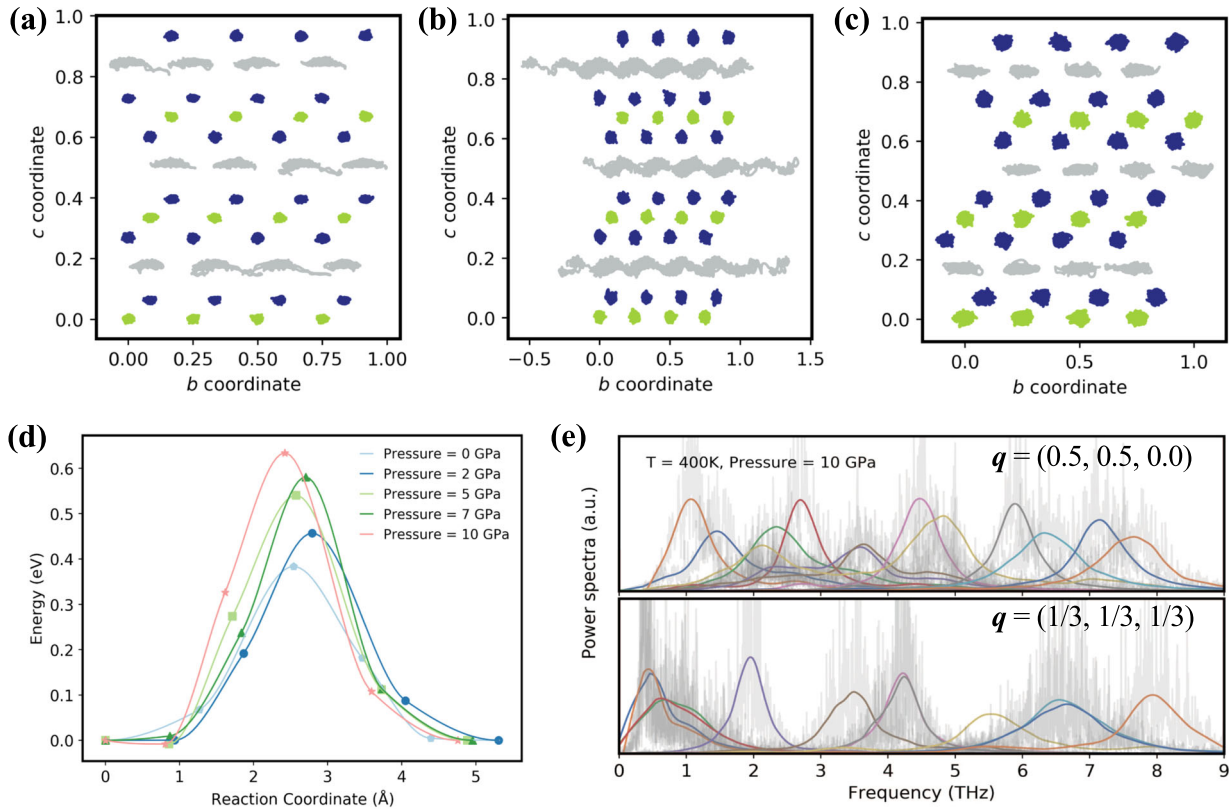
Fig. 5 Pressure response of superionic diffusion of Ag atoms. Trajectory of Ag (gray), Cr (green) and Se atoms (blue) in the *b-c* plane at **a** 300 K 0 GPa, **b** 400 K 0 GPa and **c** 400 K 10 GPa in fractional coordinate system. The figure is plotted by depicting the projection of all 192 atoms onto the *b-c* plane, sampled every 120 fs of 240 ps AIMD simulation with *NVT* ensemble. **d** The migration energy barriers of Ag atoms along two tetrahedral sites under different hydrostatic pressures, which are calculated from CI-NEB. **e** The corresponding mode-projected power spectra of AgCrSe$_2$ at *q*-vector (0.5, 0.5, 0.0) and *q*-vector (1/3, 1/3, 1/3) and the convolved data (solid curves) based on LOWESS with a bandwidth of 0.08 THz for the 12 phonon branches.

implemented in Phonopy[39], with an atomic displacement amplitude of 0.01 Å.

AIMD simulations were performed on a 192-atom $4 \times 4 \times 1$ supercell of the conventional unit cell and the duration of MD simulations was 240 ps with a 4 fs time step. A Γ point mesh combined with an energy convergence of 10^{-5} eV were applied to all AIMD simulations. Before data collection, all systems were initially relaxed by minimizing the potential energy and then equilibrated for at least 20 ps using NVT ensemble with Nose–Hoover thermostat. Unless otherwise noted, remaining AIMD parameters were kept identical to those of the harmonic phonon calculations. The ADP is defined as $\overline{u^2}$, where u is the amplitude of atomic vibrations with respect to the average positions of atoms in AIMD.

The RMSD is defined in Eq. (1):

$$\text{RMSD}(t) = \sqrt{\frac{\sum_{n=1}^{N}(r_i(t) - r_i(t_0))^2}{N}} \tag{1}$$

where N is the number of atoms and $r_i(t)$ is the position of atom i at time t. Then, the self-diffusion constant was calculated by Eq. (2):

$$D = \lim_{t \to \infty} \frac{1}{6t}(\text{RMSD}(t))^2 \tag{2}$$

In order to calculate the anharmonic power spectra, the dynamical matrix was obtained from the small displacement method as implemented in Phonopy[39], which was then diagonalized to give the normal mode phonon eigenvectors. The mode-projected power spectra were calculated by projecting the atomic velocities onto the phonon eigenvectors using the normal-mode-decomposition technique[40,41], which enables us to disentangle phonon modes with similar frequencies in such a complex system. Then, the one side mode-based power spectra

were defined as Eq. (3)

$$G_{q,s}(\omega) = 2 \int_{-\infty}^{+\infty} \langle v_{q,s}^*(0) v_{q,s}(\tau) \rangle e^{i\omega\tau} d\tau \tag{3}$$

where q is the wave vector, s is the mode polarization vector and $\langle v_{q,s}^*(0) v_{q,s}(\tau) \rangle$ is the autocorrelation function of $v_{q,s}(t)$ from AIMD simulations defined as Eq. (4)

$$\langle v_{q,s}^*(0) v_{q,s}(\tau) \rangle = \lim_{t' \to \infty} \frac{1}{t'} \int_0^{t'} v_{q,s}(t+\tau) v_{q,s}^*(t) dt \tag{4}$$

Then, the Lorentzian function was applied to fit $G_{q,s}(\omega)$:

$$G_{q,s}(\omega) \approx \frac{\langle |v_{q,s}(t)|^2 \rangle}{\frac{1}{2}\gamma_{q,s}\pi\left(1 + \left(\frac{\omega - \widetilde{\omega}_{q,s}}{\frac{1}{2}\gamma_{q,s}}\right)^2\right)} \tag{5}$$

where $\widetilde{\omega}_{q,s}$ is determined as the peak position and the phonon linewidth $\gamma_{q,s}$ is the full width half maximum.

DATA AVAILABILITY
All data generated or analyzed during this study are included in this published article (and its supplementary information files).

REFERENCES
1. Frenkel, Y. I. *Kinetic Theory of Liquids*. (Dover, New York, 1955).

2. Trachenko, K. Heat capacity of liquids: an approach from the solid phase. *Phys. Rev. B* **78**, 104201 (2008).

3. Wachsman, E. D. & Lee, K. T. Lowering the temperature of solid oxide fuel cells. *Science* **334**, 935–939 (2011).

4. Kato, Y. et al. High-power all-solid-state batteries using sulfide superionic conductors. *Nat. Energy* **1**, 16030 (2016).

5. Bhattacharya, S. et al. High thermoelectric performance of $(AgCrSe_2)_{0.5}(CuCrSe_2)_{0.5}$ nano-composites having all-scale natural hierarchical architectures. *J. Mater. Chem. A* **2**, 17122–17129 (2014).

6. Liu, H. et al. Copper ion liquid-like thermoelectrics. *Nat. Mater.* **11**, 422 (2012).

7. Tewari, G. C., Tripathi, T., Yamauchi, H. & Karppinen, M. Thermoelectric properties of layered antiferromagnetic $CuCrSe_2$. *Mater. Chem. Phys.* **145**, 156–161 (2014).

8. Voneshen, D. et al. Suppression of thermal conductivity by rattling modes in thermoelectric sodium cobaltate. *Nat. Mater.* **12**, 1028 (2013).

9. Koza, M. M. et al. Breakdown of phonon glass paradigm in La- and Ce-filled Fe_4Sb_{12} skutterudites. *Nat. Mater.* **7**, 805 (2008).

10. Biswas, K. et al. High-performance bulk thermoelectrics with all-scale hierarchical architectures. *Nature* **489**, 414 (2012).

11. Rowe, D. M. *Conversion Efficiency and Figure-of-Merit* (CRC press, 1995).

12. Li, B. et al. Liquid-like thermal conduction in intercalated layered crystalline solids. *Nat. Mater.* **17**, 226 (2018).

13. Damay, F. et al. Localised Ag^+ vibrations at the origin of ultralow thermal conductivity in layered thermoelectric $AgCrSe_2$. *Sci. Rep.* **6**, 23415 (2016).

14. Wakamura, K., Miura, F., Kojima, A. & Kanashiro, T. Observation of anomalously increasing phonon damping constant in the β phase of the fast-ionic conductor Ag_3Si. *Phys. Rev. B* **41**, 2758 (1990).

15. Wakamura, K., Hirokawa, K. & Orita, K. Observation of characteristic phonon spectra for cage and mobile ions in the layered superionic conductor $AgCrS_2$. *J. Phys. Chem. Solids* **57**, 75–80 (1996).

16. Niedziela, J. L. et al. Selective breakdown of phonon quasiparticles across superionic transition in $CuCrSe_2$. *Nat. Phys.* **15**, 73 (2019).

17. Gagor, A., Gnida, D. & Pietraszko, A. Order-disorder phenomena in layered $CuCrSe_2$ crystals. *Mater. Chem. Phys.* **146**, 283–288 (2014).

18. Bhattacharya, S. et al. $CuCrSe_2$: A high performance phonon glass and electron crystal thermoelectric material. *J. Mater. Chem. A* **1**, 11289–11294 (2013).

19. Murphy, D., Chen, H. & Tell, B. Superionic conduction in $AgCrS_2$ and $AgCrSe_2$. *J. Electrochem. Soc.* **124**, 1268–1271 (1977).

20. Gascoin, F. & Maignan, A. Order-disorder transition in $AgCrSe_2$: a new route to efficient thermoelectrics. *Chem. Mater.* **23**, 2510–2513 (2011).

21. Wu, D. et al. Revisiting $AgCrSe_2$ as a promising thermoelectric material. *Phys. Chem. Chem. Phys.* **18**, 23872–23878 (2016).

22. Tadano, T., Gohda, Y. & Tsuneyuki, S. Impact of rattlers on thermal conductivity of a thermoelectric clathrate: a first-principles study. *Phys. Rev. Lett.* **114**, 095501 (2015).

23. Pailhès, S. et al. Localization of propagative phonons in a perfectly crystalline solid. *Phys. Rev. Lett.* **113**, 025506 (2014).

24. Zhang, D. -B., Sun, T. & Wentzcovitch, R. M. Phonon quasiparticles and anharmonic free energy in complex systems. *Phys. Rev. Lett.* **112**, 058501 (2014).

25. Chen, Y., Ai, X. & Marianetti, C. A. First-principles approach to nonlinear lattice dynamics: anomalous spectra in PbTe. *Phys. Rev. Lett.* **113**, 105501 (2014).

26. Sun, T., Shen, X. & Allen, P. B. Phonon quasiparticles and anharmonic perturbation theory tested by molecular dynamics on a model system. *Phys. Rev. B* **82**, 224304 (2010).

27. Sun, T., Zhang, D. -B. & Wentzcovitch, R. M. Dynamic stabilization of cubic $CaSiO_3$ perovskite at high temperatures and pressures from ab initio molecular dynamics. *Phys. Rev. B* **89**, 094109 (2014).

28. Wang, C., Liu, Y., Liu, S. F., Li, B. & Chen, Y. Giant phonon tuning effect via pressure-manipulated polar rotation in perovskite $MAPbI_3$. *J. Phys. Chem. Lett.* **9**, 3029–3034 (2018).

29. Kittel, C. *Introduction to Solid State Physics*. (Wiley, New York, 1996).

30. Kim, H. et al. Ultralow thermal conductivity of β-Cu_2Se by atomic fluidity and structure distortion. *Acta Mater.* **86**, 247–253 (2015).

31. Momma, K. & Izumi, F. *VESTA 3* for three-dimensional visualization of crystal, volumetric and morphology data. *J. Appl. Crystallogr.* **44**, 1272–1276 (2011).

32. Merritt, E. A. Expanding the model: anisotropic displacement parameters in protein structure refinement. *Acta Crystallogr. D Biol. Crystallogr.* **55**, 1109–1117 (1999).

33. Ding, J. et al. Anharmonic lattice dynamics and superionic transition in $AgCrSe_2$. *Proc. Natl Acad. Sci. U.S.A.* **117**, 3930–3937 (2020).

34. Gascoin, F. & Maignan, A. Order-disorder transition in $AgCrSe_2$: a new route to efficient thermoelectrics. *Chem. Mater.* **23**, 2510–2513 (2011).

35. Henkelman, G. & Jónsson, H. Improved tangent estimate in the nudged elastic band method for finding minimum energy paths and saddle points. *J. Chem. Phys.* **113**, 9978–9985 (2000).

36. Kresse, G. & Hafner, J. Ab initio molecular dynamics for liquid metals. *Phys. Rev. B* **47**, 558 (1993).

37. Perdew, J. P., Burke, K. & Ernzerhof, M. Generalized gradient approximation made simple. *Phys. Rev. Lett.* **77**, 3865 (1996).

38. Blöchl, P. E. et al. Projector augmented-wave method. *Phys. Rev. B* **50**, 17953 (1994).

39. Togo, A. & Tanaka, I. First principles phonon calculations in materials science. *Scr. Mater.* **108**, 1–5 (2015).

40. Carreras, A., Togo, A. & Tanaka, I. DynaPhoPy: a code for extracting phonon quasiparticles from molecular dynamics simulations. *Comput. Phys. Commun.* **221**, 221–234 (2017).

41. McGaughey, A. & Larkin, J. M. Predicting phonon properties from equilibrium molecular dynamics simulations. *Ann. Rev. Heat Transfer* **17**, 49–87 (2014).

ACKNOWLEDGEMENTS

AUTHOR CONTRIBUTIONS

Y.C. proposed and supervised the investigation. C.W. and Y.C. implemented the method and analyzed the results. C.W. and Y.C. wrote the manuscript.

COMPETING INTERESTS

The authors declare no competing interests.

ADDITIONAL INFORMATION

Supplementary information is available for this paper at https://doi.org/10.1038/s41524-020-0295-8.

Correspondence and requests for materials should be addressed to Y.C.

Reprints and permission information is available at http://www.nature.com/reprints

Publisher's note Springer Nature remains neutral with regard to jurisdictional claims in published maps and institutional affiliations.